Ultrasound in Med. & Biol., Vol. ■, No. ■, pp. 1–13, 2010

0301-5629/$ - see front matter

ELSEVIER

doi:10.1016/j.ultrasmedbio.2010.08.015

● *Original Contribution*

NONLINEAR SHELL BEHAVIOR OF PHOSPHOLIPID-COATED MICROBUBBLES

Marlies Overvelde,* Valeria Garbin,*[1] Jeroen Sijl,* Benjamin Dollet,*[2] Nico de Jong,*† Detlef Lohse,* and Michel Versluis*

*Physics of Fluids Group, Research Institute for Biomedical Technology and Technical Medicine MIRA, University of Twente, Enschede, The Netherlands; and †Biomedical Engineering, Erasmus MC, Rotterdam, The Netherlands

(*Received* 5 *March* 2010; *revised* 21 *August* 2010; *in final form* 27 *August* 2010)

Abstract—The influence of the stabilizing phospholipid-coating on the nonlinear dynamics of ultrasound contrast agent microbubbles is investigated. We record the radial dynamics of individual microbubbles with an ultra high-speed camera as a function of both driving pressure and frequency. The viscoelastic shell was found to enhance the nonlinear bubble response at acoustic pressures as low as 10 kPa. For increasing acoustic pressures a decrease of the frequency of maximum response was observed for a distinct class of bubbles, leading to a pronounced skewness of the resonance curve, which we show to be the origin of the "thresholding" behavior (Emmer et al. 2007). For the other bubbles, the frequency of maximum response was found to lie just above the resonance frequency of an uncoated microbubble and to be independent of the applied acoustic pressure. The shell-buckling bubble model (Marmottant et al. 2005), which accounts for buckling and rupture of the shell, captures both cases for a unique set of the shell parameters, the relevant parameter being the phospholipid concentration at the bubble interface. (E-mail: m.versluis@utwente.nl) © **2010 World Federation for Ultrasound in Medicine & Biology.**

Key Words: **Ultrasound contrast agents, Microbubbles, Resonance, Nonlinear bubble dynamics, Phospholipid coating.**

INTRODUCTION

Ultrasound is the most commonly used medical imaging technique. Compared with computed tomography (CT) and magnetic resonance imaging (MRI) ultrasound offers the advantage that the hardware is relatively inexpensive and that it provides real-time images. Imaging with ultrasound is based on the reflection of the transmitted sound wave at tissue interfaces, where the wave encounters an acoustic impedance mismatch and scattering due to inhomogeneities in the tissue. Unlike tissue, blood cells are poor ultrasound scatterers, resulting in a low contrast echo. To enhance the visibility of the blood pool, ultrasound contrast agents (UCA) have been developed, enabling the visualization of the perfusion of organs. A promising new application of UCA is in molecular imaging with ultrasound (Lindner et al. 2000; Lindner 2004) and in localised drug delivery (Unger et al. 2001; Klibanov 2006).

A typical UCA is composed of a suspension of microbubbles (radius 1–5 μm), which are coated with a phospholipid, albumin or polymer shell. The coating decreases the surface tension σ and, therefore, the capillary pressure $2\sigma/R$ and in addition counteracts diffusion through the interface, thus preventing the bubble from quickly dissolving in the blood. The mechanism by which microbubbles enhance the contrast in ultrasound medical imaging is two-fold. First, microbubbles reflect ultrasound more efficiently than tissue due to the larger difference in acoustic impedance with their surroundings. Second, in response to the oscillating pressure field microbubbles undergo radial oscillations due to their compressibility, which in turn generates a secondary sound wave. The oscillations can be highly nonlinear and, likewise, so is the sound emitted by the oscillating bubbles. Several pulse-echo techniques have been developed to increase the contrast-to-tissue ratio (CTR), making use of the nonlinear components in the acoustic response of microbubbles, which are not found in the tissue, *e.g.* pulse-inversion (Hope Simpson et al. 1999)

Address correspondence to: Michel Versluis, Physics of Fluids Group, University of Twente, PO Box 217, 7500 AE Enschede, The Netherlands. E-mail: m.versluis@utwente.nl

[1] Present address: Department of Chemical and Biomolecular Engineering, University of Pennsylvania, 330 South 33rd St., Philadelphia PA 19104, USA.

[2] Present address: Institut de Physique de Rennes, UMR UR1-CNRS 6251, Université Rennes 1, Bâtiment 11A, 35042 Rennes Cedex, France.

and power modulation (Brock-Fisher et al. 1996). The nonlinear response specific to coated microbubbles offers the potential for new strategies for the optimization of the CTR.

The bubble dynamics in an ultrasound field can be described by a Rayleigh-Plesset type equation (Plesset and Prosperetti 1977; Brenner et al. 2002). The influence of the coating has been investigated in the last two decades, resulting in various extensions of the Rayleigh-Plesset equation. De Jong et al. (1994) describe the coating as a thin homogeneous viscoelastic solid with a shell elastic parameter S_p and a shell friction parameter S_f. A more theoretical approach was provided by (Church 1995) who considered a viscoelastic surface layer of finite thickness. The models by De Jong et al. and Church were both developed for the albumin-coated contrast agent Albunex. Hoff et al. (2000) reduced the model developed by Church to the limit of a thin shell. Sarkar et al. (2005) proposed a model for a thin shell of a viscoelastic solid where the effective surface tension depends on the area of the bubble and the elasticity of the shell. In the model by Stride (2008), the coating is a molecular monolayer, which is treated as a viscoelastic homogeneous material and the shell parameters depend on the surface molecular concentration. Doinikov and Dayton (2007) addressed the lipid shell as a viscoelastic fluid of finite thickness described by the linear Maxwell constitutive equation.

The models accounting for a viscoelastic solid predict that the elasticity of the shell increases the resonance frequency. Van der Meer et al. (2007) scanned the insonation frequency at constant acoustic pressure to obtain resonance curves. The acoustic pressure was maintained below 40 kPa to ensure linear bubble dynamics. Van der Meer et al. (2007) indeed found an increase of the resonance frequency with respect to uncoated microbubbles.

Emmer et al. (2007) investigated the nonlinear dynamics of phospholipid-coated microbubbles $R_0 = 1-5\,\mu$m by increasing the applied acoustic pressure at a constant frequency of 1.7 MHz. They found that a threshold pressure exists, for microbubbles smaller than $R_0 = 2\,\mu$m, for the onset of bubble oscillations and that the threshold pressure decreases with increasing bubble size. Bubbles with a radius larger than 2 μm show a linear increase in the amplitude of oscillation with the applied acoustic pressure.

De Jong et al. (2007) observed another nonlinear phenomenon which was termed "compression-only" behavior, where the coated bubbles compress significantly more than they expand. In the study of De Jong et al. (2007), "compression-only" behavior was observed in 40 out of 100 experiments on phospholipid-coated bubbles, for acoustic pressures as low as 50 kPa. "Compression-only" behavior was most pronounced for small bubbles. Models accounting for a linear viscoelastic shell do not predict the "thresholding" or the "compression-only" behavior.

Marmottant et al. (2005) developed a model that incorporates the viscoelastic shell and in addition accounts for buckling and rupture of the shell that predicts the "compression-only" behavior in great detail. The model is based on the behavior of a phospholipid monolayer for quasi-static compression (Crane and Hall 2001; Borden and Longo 2002; Pocivavsek et al. 2008). Depending on the number of phospholipid molecules per unit area the gas-water interface is shielded to a different extent, resulting in a different effective surface tension. In a small range of expansion and compression, the phospholipid-shell behaves elastically as in the previous models and the effective surface tension is linear with the surface area of the bubble. In the elastic regime, compression of the bubble decreases the surface area and, assuming a constant number of phospholipids, thus, increases the packing density and decreases the effective surface tension. For further compression, the bubble reaches a critical phospholipid packing density where the dense phospholipid monolayer starts to buckle. Below the buckling radius, the effective surface tension vanishes. On the other hand, expansion of the bubble results in a lower packing density. Above a critical radius for the expansion, the concentration of the phospholipids at the interface is so low that the monolayer ruptures. If the gas is in direct contact with the liquid, the effective surface tension reaches the surface tension of the water-gas interface.

Single bubbles were characterized by scanning in a systematic way, one single control parameter. Van der Meer et al. (2007) scanned the frequency, resulting in the resonance curve of the bubble. Emmer et al. (2007) scanned the driving pressure resulting in the observation of the "thresholding" behavior for the smaller bubbles. While the "thresholding" behavior has remained unexplained until now and it is well known that the resonance curve becomes asymmetrical with increasing acoustic pressure (Prosperetti 1975; Lauterborn 1976), a better insight in the nonlinear phenomena of coated bubbles can possibly be gained from a full parameter study where we scan in a single bubble experiment both the applied acoustic pressure and the insonation frequency.

In this article, we measure the resonance curve of a bubble as a function of the acoustic pressure to study the influence of the acoustic pressure on the resonance curve. Similarly, we study the influence of the frequency on the "thresholding" behavior. The experimental results are compared with the existing models and the influence of the phospholipid-coating on the nonlinear dynamics of UCA microbubbles is discussed in detail.

METHODS

Models

A useful description of the radial dynamics of a coated bubble is given by an extended Rayleigh-Plesset equation (Marmottant et al. 2005):

$$\rho\left(\ddot{R}R+\frac{3}{2}\dot{R}^2\right)=\left(P_0+\frac{2\sigma(R_0)}{R_0}\right)\left(\frac{R_0}{R}\right)^{3\kappa}\left(1-\frac{3\kappa\dot{R}}{c}\right)-P_0-P(t)-4\mu\frac{\dot{R}}{R}-\frac{2\sigma(R)}{R}-4\kappa_s\frac{\dot{R}}{R^2} \quad (1)$$

where ρ is the liquid density, μ the dynamic viscosity of the liquid, c the speed of sound in the liquid and κ the polytrophic exponent of the gas inside the bubble (we use $\kappa=1.07$ for C_4F_{10}). P_0 is the ambient pressure and $P(t)$ is the driving pressure pulse with a pressure amplitude P_a. R_0 is the initial bubble radius, $R(t)$ the time-dependent radius of the bubble and the overdots denote the time derivatives. κ_s accounts for the surface dilatational viscosity of the shell and $\sigma(R)$ is the effective surface tension which in some models is a function of the radius.

In this section, we discuss the results of three different models: a model for an uncoated bubble, a model for a bubble with a linear viscoelastic shell and a model including buckling and rupture of the shell. In the case of an uncoated bubble, there is no shell and the surface viscosity is $\kappa_s=0$. The gas is in direct contact with the water, resulting in the surface tension of the gas-liquid system $\sigma(R)=\sigma_w$.

The shell-buckling model by Marmottant et al. (2005) accounts for three regimes of the shell behavior: elastic, buckled and ruptured and the model is applicable to high amplitude oscillations. Figure 1 shows the effective surface tension in the three regimes which is given by:

$$\sigma(R)=\begin{cases}0 & \text{if } R\leq R_b \text{ (buckled)}\\ \chi\left(\frac{R^2}{R_b^2}-1\right) & \text{if } R_b<R<R_r \text{ (elastic)}\\ \sigma_w & \text{if } R\geq R_r \text{ (ruptured)}\end{cases} \quad (2)$$

with χ the elasticity of the shell and σ_w the surface tension of the gas-water interface. The shell buckles for radii below the buckling radius R_b and is in the ruptured state for radii larger than $R_r=R_b\sqrt{\frac{\sigma_w}{\chi}+1}$. The effective surface tension in the elastic regime depends on the concentration of phospholipids and therefore on the area of the bubble. The initial state is defined by the initial surface tension $\sigma(R_0)$, which is directly related to the buckling radius $R_b=R_0/\sqrt{\frac{\sigma(R_0)}{\chi}+1}$, see Figure 1. We prefer to define $\sigma(R_0)$ instead of R_b as was done by Marmottant et al. (2005) because $\sigma(R_0)$ immediately reveals the initial state of the shell with respect to the buckled and ruptured regime.

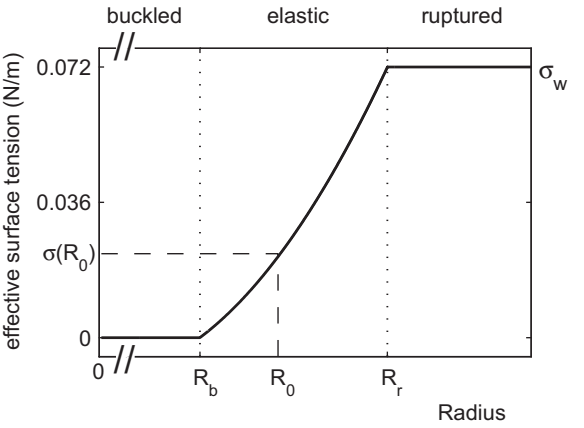

Fig. 1. Effective surface tension in the shell-buckling model as a function of the bubble radius. The effective surface tension in the model has three regimes. The bubble buckles for $R \leq R_b$, is ruptured for $R \geq R_r$ and behaves elastically for $R_b < R < R_r$.

The results will also be compared with a coated bubble model accounting for a linear viscoelastic shell, which is valid in the limit of small amplitude oscillations. We use the linearized effective surface tension of the shell-buckling model in the elastic regime:

$$\sigma(R)=\sigma(R_0)+2\chi\left(\frac{R}{R_0}-1\right) \quad (3)$$

In the case $\sigma(R_0)=\sigma_w$, we obtain the well-known equation for the effective surface tension of De Jong et al. (1994).

For small amplitude oscillations, we can obtain the eigenfrequency of the bubble. For a coated bubble, the eigenfrequency of the bubble with a linear viscoelastic shell equals the eigenfrequency of the model by Marmottant et al. (2005) in the elastic regime. The eigenfrequency of a bubble with a linear viscoelastic shell f_0^{coated} is given by Van der Meer et al. (2007):

$$f_0^{coated}=\frac{1}{2\pi}\sqrt{\frac{1}{\rho R_0^2}\left(3\kappa P_0+(3\kappa-1)\frac{2\sigma(R_0)}{R_0}+\frac{4\chi}{R_0}\right)} \quad (4)$$

In the case of an uncoated bubble, the eigenfrequency is (Plesset and Prosperetti 1977; Hilgenfeldt et al. 1998):

$$f_0^{uncoated}=\frac{1}{2\pi}\sqrt{\frac{1}{\rho R_0^2}\left(3\kappa P_0+(3\kappa-1)\frac{2\sigma_w}{R_0}\right)} \quad (5)$$

The damping of the system has a negligible effect on the resonance frequency and we assume that the resonance frequency equals the eigenfrequency of the bubble.

To investigate the dynamics as a function of the applied frequency and acoustic pressure, simulations were performed for a bubble with a radius of $R_0=3.2\,\mu$m

with the three different models described above. Figure 2 shows the resonance curves obtained from numerical simulations as a function of the acoustic pressure for an uncoated microbubble (A), a microbubble with a linear viscoelastic shell (B) and a microbubble with a viscoelastic shell including buckling and rupture of the shell (C). To assure the linearity of the resonance curves, the relative fundamental amplitude of oscillation A_1 is divided by the acoustic pressure P_a. This normalization with the acoustic pressure results in identical resonance curves at each pressure in case of linear bubble dynamics. For all three models, the value A_1/P_a is normalized to the response of an uncoated bubble at $P_a=1$ kPa. The uncoated bubble has a resonance frequency near 1 MHz, see Figure 2A. The maximum amplitude $(A_1/P_a)_{norm}$ slightly decreases with increasing pressure, which reflects the onset of its nonlinear behavior.

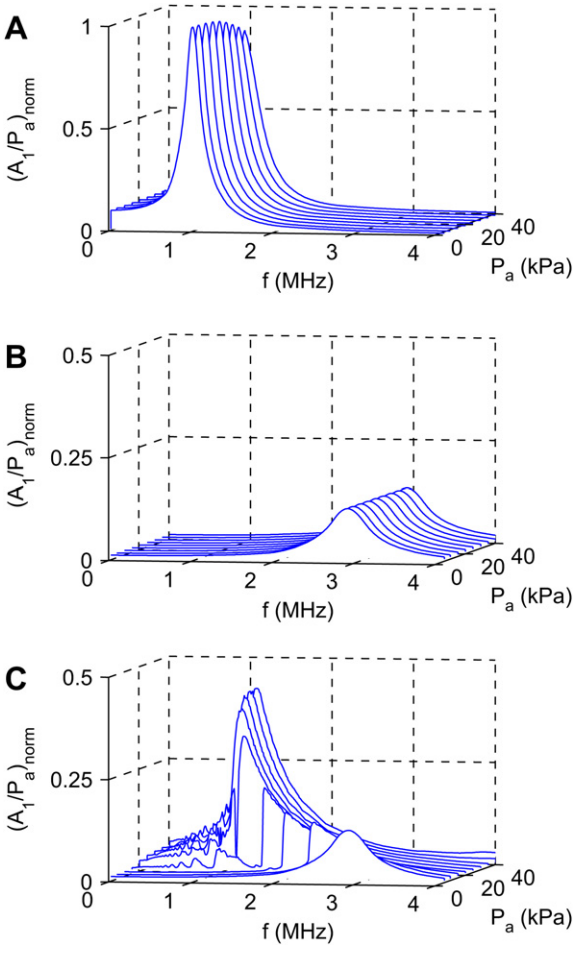

Fig. 2. Simulations of the resonance curve as a function of the acoustic pressure. The relative amplitude of oscillation A_1 is divided by the acoustic pressure amplitude P_a and normalized with the response of the uncoated bubble at $P_a=1$ kPa. (A) Uncoated. (B) Linear viscoelastic shell. (C) Elastic shell including buckling and rupture of the shell. The initial radius of the bubble is $R_0=3.2\,\mu$m and in case of a coating $\chi=2.5$ N/m, $\sigma(R_0)=0.02$ N/m and $\kappa_s=6\cdot10^{-9}$ kg/s.

In Figure 2B, the response of a bubble with the linear viscoelastic shell is shown. In the simulations, the shell elasticity $\chi=2.5$ N/m, the shell viscosity $\kappa_s=6\cdot10^{-9}$ kg/s and the initial effective surface tension $\sigma(R_0)=0.02$ N/m. The resonance frequency of the bubble with a purely viscoelastic coating is almost three times the resonance frequency of the uncoated bubble, owing to the increased elasticity while the maximum amplitude of oscillation is eight times lower than that of the uncoated bubble as a result of the combined effect of the increased damping and elasticity of the shell. The oscillation amplitude is independent of the applied acoustic pressure and indicates a linear response.

Figure 2C shows the simulations performed with the shell-buckling model, showing dependence on the applied acoustic pressure. To compare the simulations with the results of the purely viscoelastic shell, the shell parameters are identical to the shell parameters in Figure 2B. For low acoustic pressure $P_a=1$ kPa, the bubble is oscillating in the elastic regime. Therefore, the resonance curve is identical to the response of the bubble with the linear viscoelastic shell. An increase of the acoustic pressure induces strong nonlinear behavior and skewing of the resonance curves is observed. For linear oscillations, the response is maximal at the resonance frequency while in the general case of nonlinear behavior the maximum response is found at the frequency of maximum response, which in the present case, decreases with increasing acoustic pressure. At $P_a=40$ kPa, the frequency of maximum response decreased and approaches the eigenfrequency of the uncoated bubble. The relative amplitude of oscillation at the frequency of maximum response increases with increasing acoustic pressure, which reveals another nonlinear response. The resonance behavior obtained with the three models is significantly different. An experimental study of the resonance curves as a function of the acoustic pressure applied to UCA microbubbles may, therefore, reveal the influence of the phospholipid-coating on the bubble dynamics.

Experimental set-up

Figure 3 shows a schematic drawing of the experimental set-up. The ultrasound contrast agent BR-14 (Bracco S.A., Geneva, Switzerland) was injected in an OptiCell filled with a saline solution. The OptiCell chamber was mounted in a water bath and connected to a three-dimensional (3-D) micropositioning stage. A water tank mounted on a planar-stage was designed to hold an illumination fiber and the ultrasound transducer (PA168; Precision Acoustics, Dorchester, United Kingdom). The driving pulse for the transducer was generated by an arbitrary waveform generator (Tabor

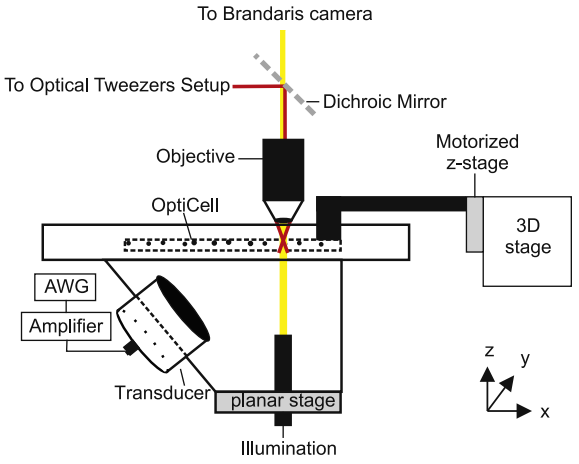

Fig. 3. Schematic drawing of the experimental set-up. The solution containing contrast agent microbubbles is injected in an OptiCell chamber. The chamber is located in a water tank, which holds the transducer and illumination fiber. The driving ultrasound pulse is produced by an arbitrary waveform generator (AWG), amplified and sent to the transducer. The bubbles are imaged and manipulated with optical tweezers through the same 100 × objective.

8026; Tabor Electronics, Tel Hanan, Israel) and amplified by an RF-amplifier (ENI 350L; Electronic Navigation Industries, Inc., Rochester, NY, USA). The sample was imaged with an upright microscope equipped with a water-immersed 100 × objective (LUMFPL; Olympus, Zoeterwoude, The Netherlands). The dynamics of the microbubble was captured with the ultra high-speed Brandaris 128 camera (Chin et al. 2003) at a frame rate of 15 million frames per second (Mfps). An optical tweezers set-up allowed for the positioning of a single microbubble in 3-D (Garbin et al. 2005). The infrared laser beam of the optical tweezers was coupled into the microscope using a dichroic mirror. The optical trap was formed through the imaging objective. The set-up combining the Brandaris 128 camera with optical tweezers is described in detail by Garbin et al. (2007).

The bubbles were insonified with an ultrasound burst of 10 cycles whose first and last 3 cycles were tapered with a Gaussian envelope. To scan the frequency with a constant acoustic pressure, the transducer was calibrated prior to the experiments with a needle hydrophone (HPM02/1; Precision Acoustics, Dorchester, United Kingdom). To align the acoustical focus of the transducer and the optical focus of the objective, the OptiCell was removed, the tip of the hydrophone was positioned in the focus of the objective and the transducer was aligned with the planar-stage. The material of the OptiCell is nearly acoustically transparent. On the other hand, small reflections at the OptiCell wall may change the local pressure field. The 3-D stage connected to the OptiCell chamber allowed for the movement of the sample independently of the transducer to keep the acoustical and optical focus aligned. A motorized stage (M110-2.DGm; Physik Instrumente [PI], Karlsruhe, Germany) was used to accurately control the distance between the bubble in the trap and the OptiCell wall. In all experiments, the minimum distance between the bubble and the wall was 100 μm.

The experimental protocol is based on the microbubble spectroscopy method described by Van der Meer et al. (2007). Each resonance curve is a result of 2 runs of the Brandaris 128 camera recording six movies of 128 frames with 12 increasing frequencies at constant acoustic pressure. The experiment was repeated several times for increasing acoustic pressure on the very same bubble, until the full parameter space of acoustic pressure and frequency ranges was covered (typically 8 pressures). Each one of the 96 (8 × 12) movies therefore captured the radial dynamics at a single acoustic pressure and frequency. The radius vs. time curve ($R(t)$-curve) of the bubble was determined by tracking the contour of the bubble in each frame with a code programmed in Matlab®.

To ensure that the observed nonlinear phenomena were not caused by changes in the bubble properties due to repeated insonation, we performed a set of control experiments. In the first control experiment, we sent 12 pulses at constant acoustic pressure and frequency and confirmed the reproducibility of the 12 $R(t)$-curves. The same protocol was then repeated for a higher acoustic pressure and we found that the relative standard deviation at the fundamental frequency was below 7% unless a bubble visibly reduced in size during the experiments. All results where any sign of shrinkage of the bubbles was observed were not considered in the present analysis.

Figure 4 shows the reproducibility of the bubble frequency response of a 2.4 μm radius bubble insonified 12 times with an acoustic pressure P_a=30 kPa and frequency f=1.7 MHz. The second test consisted in repeating a measurement of the resonance curve on a single bubble at a fixed acoustic pressure, to verify that the bubble behavior would not change due to

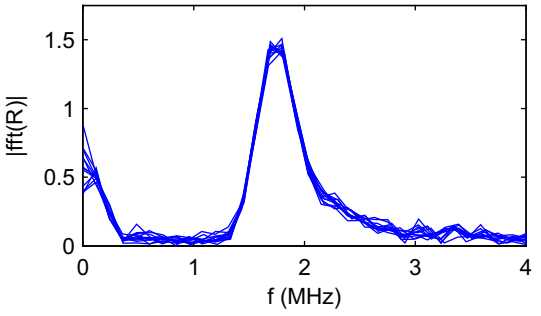

Fig. 4. The frequency response of a single 2.4 μm radius bubble insonified with P_a=30 kPa and f=1.7 MHz is reproducible over 12 separate experiments.

repetitive insonation. We observed that the frequency of maximum response was constant for a given acoustic pressure. Finally, to ensure that by repetitive frequency scans at increasing acoustic pressures the bubble properties were not altered, we repeated one run with low acoustic pressure after a few runs with increasing acoustic pressure and compared the response with the one obtained in a previous run at the same pressure. These experiments confirmed that the observed nonlinear phenomena are a result of the phospholipid-coated bubble dynamics and not a side effect due to aging of the bubble.

Figure 5A shows a typical oscillation of a $R_0=2\,\mu$m bubble insonified at a frequency $f=1.7$ MHz and at an acoustic pressure $P_a=37.5$ kPa (blue). The amplitude of the compression phase of the oscillations is larger than the expansion phase. This "compression-only" behavior (De Jong et al. 2007) causes a low frequency component (Sijl et al. 2010b). Sijl et al. (2010b) showed through a weakly nonlinear analysis that the "compression-only" behavior can be excluded by filtering out the low frequency component. Likewise, the low frequency component can be obtained by removing the higher frequency components. The relative excursion at the fundamental frequency ε_1 is shown in Figure 5B and the low frequency response in Figure 5A (red). We use as a measure for the maximum relative radial amplitude at the fundamental frequency A_1:

$$A_1=\frac{\varepsilon_1^{max}-\varepsilon_1^{min}}{2} \tag{6}$$

where ε_1^{max} is the maximum relative expansion and ε_1^{min} the minimum relative expansion, see Figure 5B.

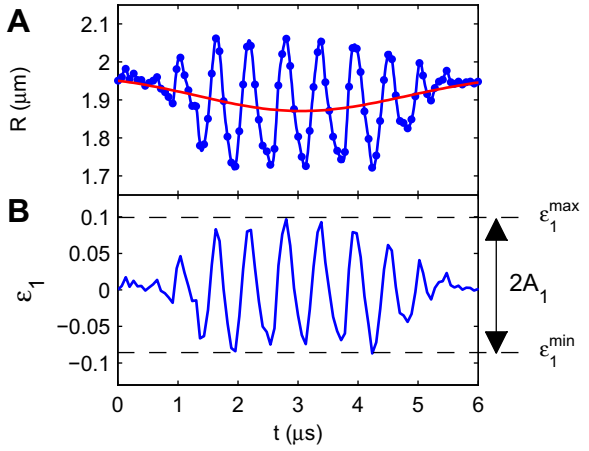

Fig. 5. A bubble with a radius $R_0=2\,\mu$m is insonified with an acoustic pressure $P_a=37.5$ kPa and a frequency $f=1.7$ MHz. (A) The experimental $R(t)$-curve (blue) and the low frequency component (red). (B) The relative fundamental response ε_1.

In the following we nondimensionalize the frequency with the eigenfrequency of the uncoated bubble:

$$\Omega=\frac{f}{f_0^{uncoated}} \tag{7}$$

and for the frequency of maximum response:

$$\Omega_{MR}=\frac{f_{MR}}{f_0^{uncoated}} \tag{8}$$

The resonance curves will be obtained from A_1 as a function of Ω.

RESULTS

Figure 6 shows the resonance curve for three values of the acoustic pressure $P_a=7.5$, 12.5 and 25 kPa. The bubble has a radius $R_0=3.2\,\mu$m and is positioned 150 μm from the wall while the applied frequency is between 0.75 and 3 MHz. The experimental data (circles) are compared

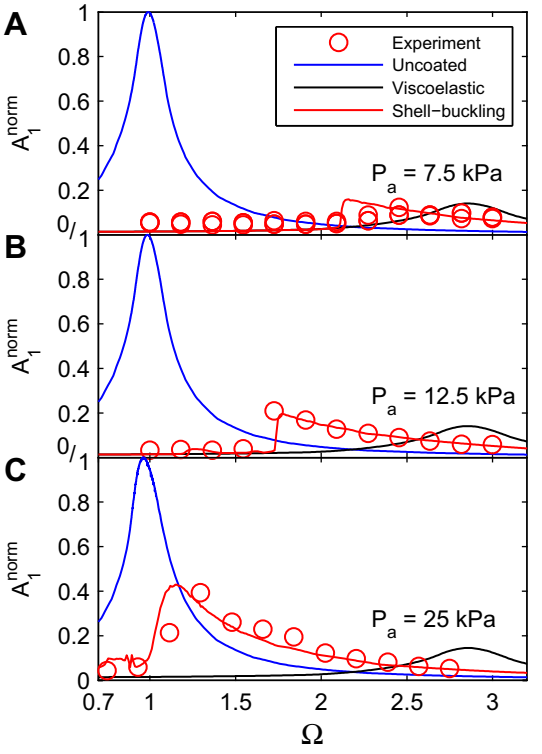

Fig. 6. Skewing of the resonance curve of a coated microbubble at low acoustic pressures [$P_a=$ 7.5 kPa (A), 12.5 kPa (B) and 25 kPa (C)]. The model for the uncoated bubble (blue) and a linear viscoelastic shell model (black) cannot predict skewing of the resonance curve at low acoustic pressures. The shell model (Marmottant et al. 2005) including buckling and rupture (red) captures the skewness of the experimental resonance curve (circles). The bubble radius is 3.2 μm and the shell parameters are the same for both coated bubble models: $\chi=2.5$ N/m, $\kappa_s=6\cdot10^{-9}$ kg/s and $\sigma(R_0)=0.02$ N/m.

with the three different models, the uncoated bubble (blue), the coated bubble with a linear viscoelastic shell (black) and the coated bubble including buckling and rupture of the shell (red). To compare the response at the three different acoustic pressures the amplitude of oscillation A_1 is normalized to the maximum simulated response of an uncoated bubble (A_1^{norm}). For an acoustic pressure P_a=7.5 kPa (A) the experimental data show a maximum response Ω_{MR}=2.5. The frequency of maximum response decreases to Ω_{MR}=1.7 at P_a=12.5 kPa (B) and to Ω_{MR}=1.4 at P_a=25 kPa (C). Besides a decrease in the frequency of maximum response the resonance curves at P_a=12.5 and 25 kPa are strongly skewed. At low acoustic pressure (P_a=7.5 kPa), the observed maximum amplitude of oscillation is small compared with the simulated amplitude of an uncoated microbubble: A_1^{norm}=0.1. The maximum amplitude of oscillation increases with increasing acoustic pressure and at P_a=25 kPa the normalized amplitude of oscillation is A_1^{norm}=0.4. The experiment at P_a=7.5 kPa was repeated to ensure that the change in behavior for increasing acoustic pressure is not an artifact due to a change in the properties of the bubble. The comparison of the experiments with the models showed that the shell-buckling model accounting for an elastic regime, buckling and rupture of the shell (red) captures the decrease in the frequency of maximum response, the asymmetry of the resonance curves and the relative amplitude of oscillation with a single set of shell parameters.

We present the experimentally obtained relative amplitude of oscillation A_1 for the full acoustic pressure and frequency scan in an iso-contour plot in Figure 7A. A total of 120 $R(t)$-curves have been measured near the frequency of maximum response Ω_{MR} in the acoustic pressure range P_a=7.5−25 kPa at an interval of 2.5 kPa. Figure 7B shows the simulations with the shell-buckling model with the same shell parameters as in Figure 6. The experimental frequency of maximum response Ω_{MR} obtained from Figure 7A (circles) is compared with simulations for the three different models in Figure 7C. Ω_{MR} decreases by 50% for an increase of the acoustic pressure from P_a=7.5 to P_a=25 kPa. The frequency of maximum response Ω_{MR} simulated with the shell-buckling model (red) is in excellent agreement with the experimental results. For comparison, the frequency of maximum response obtained with the model for an uncoated bubble and the linear viscoelastic model are shown. In the shell-buckling model at low acoustic pressures $P_a < 2$ kPa, the oscillations are in the elastic regime and the frequency of maximum response equals the resonance frequency of a coated bubble that follows from the linear viscoelastic model. Above acoustic pressures $P_a > 2$ kPa, the shell starts to buckle and the frequency of maximum response decreases rapidly, approaching the eigenfrequency of an uncoated bubble at $P_a > 20$ kPa.

A vertical scan line of Figure 7A and B results in the typical resonance curves shown in Figure 6. A horizontal scan line, on the other hand, results in the pressure-dependent response for different applied frequencies. *De facto* this is the same experiment as performed by Emmer et al. (2007) with the exception that Emmer et al. varied bubble radius R_0, not the frequency. Such a horizontal scan-line is depicted in Figure 8 where the relative amplitude of oscillation A_1 is shown for three applied frequencies Ω=2.1 (A), Ω=1.5 (B) and Ω=1 (C). For each frequency, the experimentally observed amplitude of oscillations (circles) increases nonlinearly with increasing acoustic pressure. In particular, the so-called "thresholding" behavior is apparent. The threshold pressure for the onset of oscillations depends on the frequency

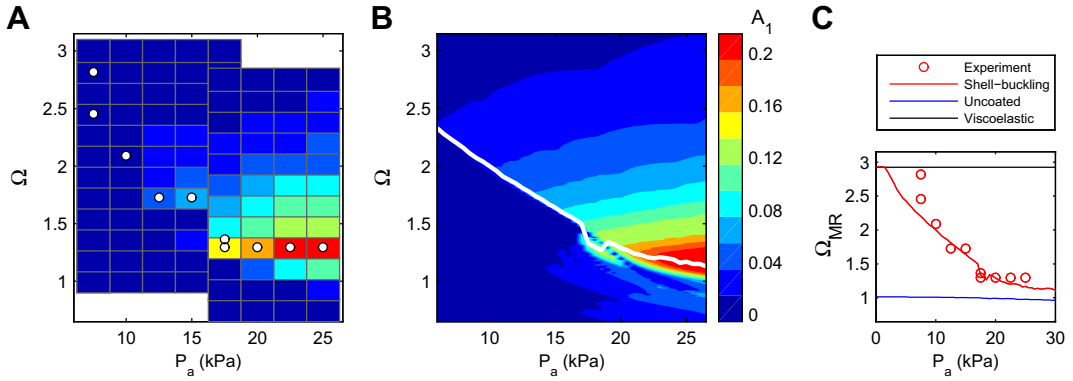

Fig. 7. The relative amplitude of oscillations A_1 as a function of the acoustic pressure P_a and frequency Ω. (A) Experimentally measured A_1 as a function of P_a and Ω for a bubble R_0=3.2 μm. The frequency of maximum response Ω_{MR} (white dots). (B) Simulations with the model including buckling and rupture of the shell. The white line shows the frequency of maximum response Ω_{MR}. The bubble has a radius of 3.2 μm and the values for the shell parameters are χ=2.5 N/m, κ_s=6·10^{-9} kg/s and $\sigma(R_0)$=0.02 N/m. (C) The frequency of maximum response Ω_{MR} as a function of P_a.

and is most pronounced for $\Omega=1.5$, where the bubble shows no oscillations if driven below $P_a=15$ kPa and abruptly starts to oscillate ($A_1 \sim 0.1$) at $P_a=17.5$ kPa. The shell-buckling model (solid lines) reproduces the data accurately and predicts the "thresholding" behavior.

The decrease of the frequency of maximum response with increasing pressure as shown in Figure 7C does not uniquely describe the response of all bubbles. We observe a different behavior for different bubbles, even for bubbles of the same size. Figure 9 shows the frequency of maximum response Ω_{MR} of two equally sized bubbles $R_0=2.4\,\mu$m. To allow for a comparison of the response of different bubbles, we plot Ω_{MR} as a function of A_1 instead of P_a. One bubble has a frequency of maximum response $\Omega_{MR}=2.2$ at $A_1=0.03$ and shows a decrease in the frequency of maximum response of 40% with increasing A_1, reaching a value of $\Omega_{MR}=1.4$ at $A_1=0.12$ (triangles). The second bubble shows very different behavior, $\Omega_{MR}=1.4$ and independent of A_1 (squares). The experimental results are compared with calculations of the frequency of maximum response simulated with the shell-buckling model. Simulations for different values of the shell elasticity and shell viscosity indicated that the observed trend in Ω_{MR} with A_1 is not changed by the shell parameters χ and κ_s. Therefore, simulations were performed with only one single free parameter, the initial phospholipid concentration expressed via the effective surface tension at rest $\sigma(R_0)$. The shell elasticity χ was taken 2.5 N/m and the shell viscosity κ_s was $6\cdot10^{-9}$ kg/s. Figure 9 shows that the way the frequency of maximum response changes with the amplitude of oscillation is well captured with two extreme values of

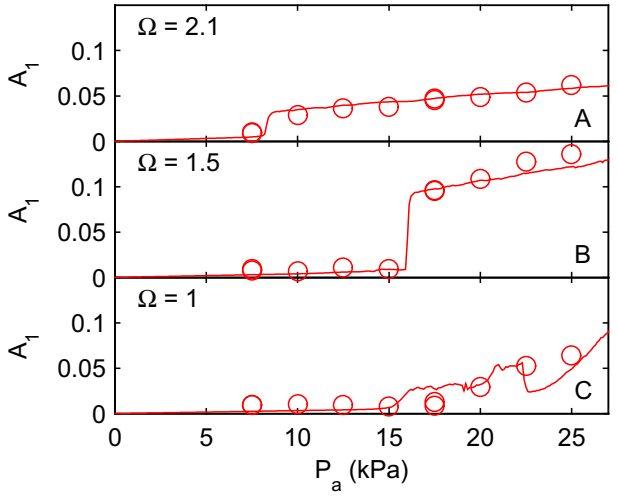

Fig. 8. Relative amplitude of oscillation A_1 as a function of the acoustic pressure P_a. A_1 increases nonlinearly and displays the "thresholding" behavior. The prediction of the shell-buckling model is plotted (lines) and captures the experimental data (circles). Shell parameters as in Fig. 7. (A) $\Omega=2.1$, (B) $\Omega=1.5$ and (C) $\Omega=1$.

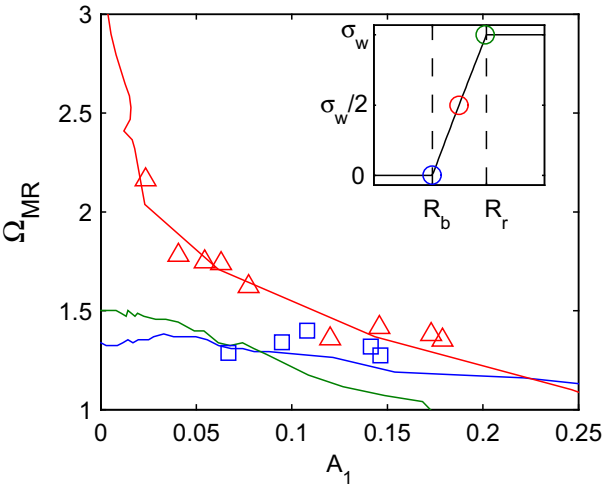

Fig. 9. Normalized frequency of maximum response Ω_{MR} as a function of the relative amplitude of oscillation A_1 for two equally sized microbubbles $R_0=2.4\,\mu$m. One of the bubbles shows a decrease in the frequency of maximum response Ω_{MR} (triangles), while the other bubble has a constant frequency of maximum response (squares). Simulations are shown with the shell-buckling model for three initial cases: the bubble is initially in the buckled state (blue), the ruptured state (green) and the elastic regime (red), see inset. The shell elasticity and shell viscosity are respectively, $\chi=2.5$ N/m, $\kappa_s=6\cdot10^{-9}$ kg/s.

the effective surface tension. Simulations for a bubble initially in the elastic state, $\sigma(R_0)=\sigma_w/2$ (red), capture the strong decrease in Ω_{MR} (triangles), while simulations for a bubble initially in the buckled state, $\sigma(R_0)=0$ N/m describe the observed constant frequency of maximum response with increasing oscillation amplitude (squares).

Over 4000 *R(t)*-curves were obtained experimentally on 45 bubbles ranging in size between $R_0=1.2-3.4\,\mu$m. The resulting 168 frequencies of maximum response Ω_{MR} are shown as a function of A_1 (dots) for all bubbles in Figure 10. For small amplitude of oscillations ($A_1 < 0.05$), the experimental data (dots) are scattered between $\Omega_{MR}=1.2$ and $\Omega_{MR}=3$. For increasing amplitude of oscillations the frequency of maximum response converges to a value of $\Omega_{MR}=1.2$.

Here, we discuss how we obtained the shell parameters. The shell elasticity was obtained from the highest frequency of maximum response at the lowest amplitude of oscillation, assuming that the shell behaves purely elastically. We should mention that strictly speaking, the simulations predict that the bubble oscillates a bit outside the elastic regime, which may result in an underestimated value for the shell elasticity. However, the shell elasticity $\chi=2.5$ N/m found is used throughout the article and results in a very good agreement for all bubble dynamics. Next, we obtained the initial surface tension for each bubble by comparing the trend in the frequency of maximum response with increasing amplitude of oscillation to the numerical simulations using different initial

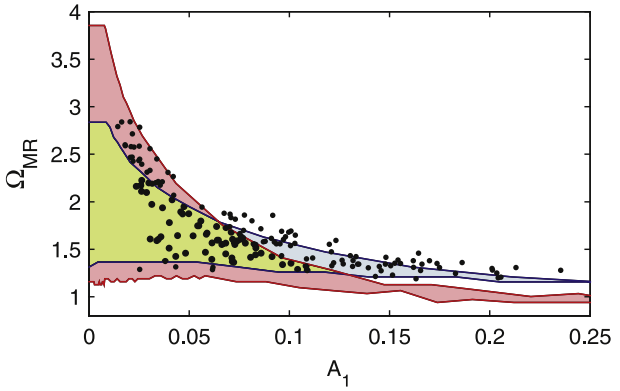

Fig. 10. Experimental obtained Ω_{MR} as a function of the relative amplitude of oscillation A_1 (dots) for all bubbles $R_0=1.2-3.4\,\mu$m. The simulated regimes of the frequency of maximum response Ω_{MR} for a small bubble $R_0=1.2\,\mu$m (red) and a large bubble $R_0=3.4\,\mu$m (blue) are plotted. The overlapping regime of both bubbles is colored green. The lines show Ω_{MR} for $\sigma(R_0)=0$ N/m (bottom) and $\sigma(R_0)=\sigma_w/2$ (top). The shell elasticity and shell viscosity are kept constant, $\chi=2.5$ N/m, $\kappa_s=6\cdot10^{-9}$ kg/s.

surface tension. Finally, we fitted the shell viscosity to match the amplitude of oscillation for all frequencies and pressures. Indeed, it was found that the full data set can be described with this single shell viscosity $\kappa_s=6\cdot10^{-9}$ kg/s. The difference between the different bubbles is caused by a small change in the initial phospholipid concentration which is expressed through the initial surface tension $\sigma(R_0)$.

Simulations of the frequency of maximum response were performed as a function of the applied acoustic pressure to vary the oscillation amplitude. The bubble sizes included were those between the smallest bubble size $R_0=1.2\,\mu$m (red) and the largest bubble size $R_0=3.4\,\mu$m (blue). The initial surface tension was varied between $\sigma(R_0)=0$ N/m and $\sigma(R_0)=\sigma_w/2$. It was found that the experimental data lie well within the boundaries set by the simulation parameters. The frequency of maximum response strongly varies at low oscillation amplitudes A_1, while for higher response $A_1 > 0.15$ the frequency of maximum response for all bubbles is practically identical and approaching the resonance frequency of an uncoated bubble. It was identified that bubble shrinkage was observed for all bubbles above an amplitude of oscillation $A_1=0.23$. Some bubbles started to shrink at an amplitude of oscillation as low as $A_1=0.1$, these results were excluded from further analysis.

DISCUSSION

Initial surface tension

In the previous section, we found a large variability in the frequency of maximum response Ω_{MR} as a function of the relative amplitude of oscillation A_1 even for equally sized bubbles. Simulations showed that the variability in the trend in Ω_{MR} can be explained by a difference in the initial surfactant concentration, expressed via the effective surface tension at rest $\sigma(R_0)$. To investigate the influence of $\sigma(R_0)$ on the "compression-only" behavior, skewing of the resonance curves and the "thresholding" behavior, we performed simulations with the shell-buckling model. The simulations were performed for a bubble with a radius $R_0=2\,\mu$m, with a shell elasticity $\chi=2.5$ N/m and a shell viscosity $\kappa_s=6\cdot10^{-9}$ kg/s.

"Compression-only" behavior was first observed in experiments by De Jong et al. (2007). Marmottant et al. (2005) showed that the initial state of the bubble, *i.e.* the initial surface tension $\sigma(R_0)$, is essential to determine whether "compression-only" behavior appears. They showed that the most pronounced "compression-only" behavior is observed for a bubble with a radius R_0 close to its buckling radius R_b, which is equivalent to $\sigma(R_0)=0$ N/m. The authors pointed out that the compression modulus $-V\frac{dP}{dV}$ of the coated bubble is much higher in the elastic state than in the buckled or ruptured state. In our simulations, the shell elasticity $\chi=2.5$ N/m and, indeed, the compression modulus of the bubble is 10 times higher in the elastic regime. Figure 11 shows the simulated bubble dynamics for a 'ruptured' bubble $\sigma(R_0)=\sigma_w$ (top), an "elastic" bubble $\sigma(R_0)=\sigma_w/2$ (middle) and a "buckled" bubble $\sigma(R_0)=0$ N/m (bottom), see also inset Figure 9. The *R(t)*-curves (A) are divided in the fundamental response ε_1 (B) and the low frequency response ε_0 (C). The low frequency response is a measure for the "compression-only" behavior of the bubble and is obtained by removing the higher frequency components in the frequency domain of the *R(t)*-curves. The buckled bubble shows more compression than expansion as expected. The expansion of the ruptured bubble is more pronounced compared with its compression, hence, we term this behavior "expansion-only" behavior in analogy of the "compression-only" behavior for the buckled bubble. The explanation is similar to that of "compression-only" behavior. The compression modulus in the ruptured regime is much lower than in the elastic regime and for a ruptured bubble it is easier to expand than to compress. In the case of an elastic bubble, the bubble starts to oscillate in the midpoint of the elastic regime and the oscillations are symmetrical.

In our experiments, we predominantly observe "compression-only" behavior. Only occasionally ($\leq$3%), the expansion was observed to be larger than the compression. From the above simulations, we conclude that most bubbles have an initial surface tension $\sigma(R_0)=0$ N/m and, therefore, R_0 close to the buckling radius. This can be explained as a result of the capillary pressure, which forces the bubble into an equilibrium,

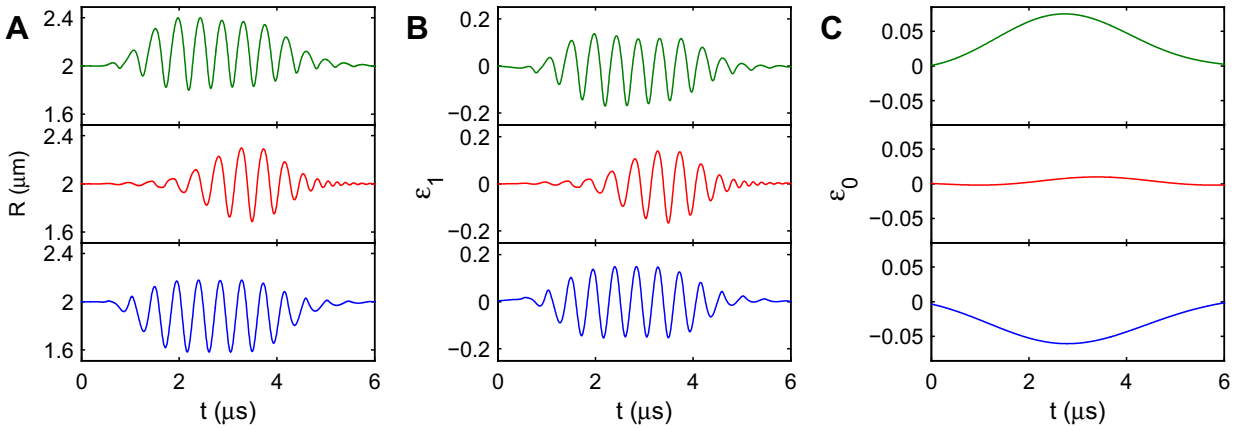

Fig. 11. Influence of the initial surface tension on the radial dynamics, $\sigma(R_0)=0$ N/m (bottom), $\sigma(R_0)=\sigma_w/2$ (middle) and $\sigma(R_0)=\sigma_w$ (top). The acoustic pressure and frequency are 40 kPa and $\Omega=1.3$, respectively. (A) $R(t)$-curve, (B) fundamental response ε_1 and (C) low frequency response ε_0.

tensionless state, as previously pointed out by Marmottant et al. (2005).

Figures 6, 7 and 8 reveal that a bubble with a skewed resonance curve shows a decrease of the frequency of maximum response with increasing acoustic pressure. In addition it displays "thresholding" behavior (Emmer et al. 2007). The initial surface tension of this particular bubble was found to be $\sigma(R_0)=0.02$ N/m. Here, we will focus on the influence of $\sigma(R_0)$ on the shape of the resonance curves and the "thresholding" behavior for the two cases most relevant to our experiments, a buckled bubble and an elastic bubble. Figure 12A shows the resonance curves for three values of the acoustic pressure $P_a=1, 20,$ and 40 kPa (top-bottom). The shape of the resonance curve of the buckled bubble (blue) is hardly changed for all three pressures. The frequency of maximum response is almost independent of the acoustic pressure and lies just above the resonance frequency of an uncoated bubble, $\Omega_{MR}=1.3$. For $P_a=1$ kPa (top) the elastic bubble (red) oscillates only in the elastic regime and behaves like a bubble modeled with a linear viscoelastic shell as can be inferred from its frequency of maximum response $\Omega_{MR}=\Omega_{res}^{coated}=3.3$. On the other hand, the frequency of maximum response Ω_{MR} of the elastic bubble decreases with increasing pressure $P_a=20$ kPa (middle). Since the radius of the elastic bubble now exceeds the elastic regime between R_b and R_r, the bubble is now also oscillating in the buckled and ruptured regime. The frequency of maximum response of the elastic bubble decreases even more for $P_a=40$ kPa (bottom), approaching the resonance frequency of an uncoated bubble. The resonance curves of the elastic bubble are strongly skewed at $P_a=20$ kPa and 40 kPa and practically no oscillations

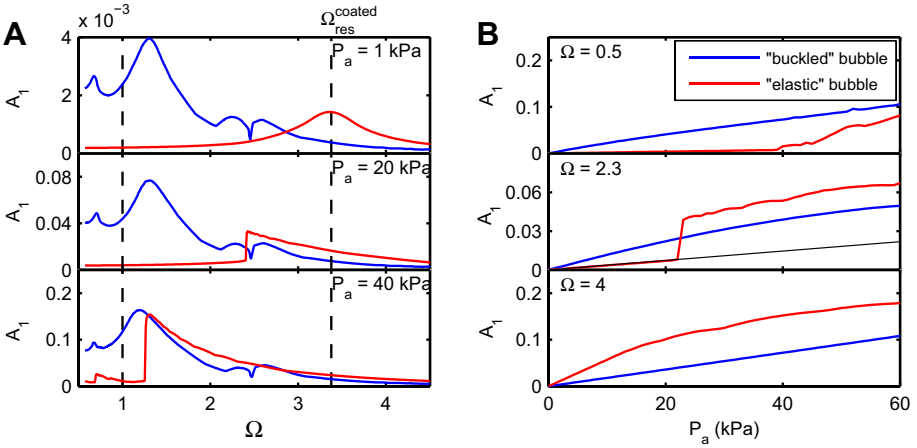

Fig. 12. Simulations for two values of the initial surface tension: $\sigma(R_0)=0$ N/m (blue) and $\sigma(R_0)=\sigma_w/2$ (red). (A) Simulated resonance curves for three values of the acoustic pressure $P_a=1$ kPa (top), $P_a=20$ kPa (middle) and $P_a=40$ kPa (bottom). (B) Simulated relative amplitude of oscillations A_1 as a function of the acoustic pressure P_a for three different applied frequencies: $\Omega=0.5$ (top), $\Omega=2.3$ (middle) and $\Omega=4$ (bottom).

are observed for frequencies below its maximum response frequency.

Figure 12B shows the influence of $\sigma(R_0)$ on the "thresholding" behavior. The amplitude of oscillations for the buckled bubble (blue) increases almost linearly with the acoustic pressure at all three frequencies (top-bottom). On the contrary, the elastic bubble (red) shows strong nonlinear behavior. For a driving frequency below the resonance frequency of the coated bubble ($\Omega_{res}^{coated}=3.3$), the amplitude of oscillations increases slowly with increasing acoustic pressure, until the slope suddenly changes and we observe "thresholding" behavior at $P_a=40$ kPa (top) or $P_a=22$ kPa (middle). The elastic bubble is initially oscillating in the elastic regime and A_1 increases very slowly with P_a. At a certain amplitude of oscillation, the bubble starts to buckle and A_1 rapidly increases with P_a, leading to an apparent "thresholding" behavior. For comparison, the linear increase in the response A_1 of a bubble with a linear viscoelastic shell is shown (black, middle).

Ambient pressure

The variability in the experimentally observed dynamics, such as skewing of the resonance curve, "thresholding" behavior and "compression-only" behavior, can be explained by a change in the initial surface tension $\sigma(R_0)$, which depends on the concentration of phospholipids at the bubble interface. Provided that the total amount of phospholipids at the interface is constant, a change in the radius of the bubble would change $\sigma(R_0)$. The extent of the elastic regime can be calculated from eqn (3) with $R=R_r, R_0=R_b, \chi=2.5$ N/m and $\sigma(R_r)-\sigma(R_b)=\sigma_w$. The total size of the elastic regime is $0.01R_0$ and a bubble with $R_0=R_b$ is only 1% smaller than a bubble starting to oscillate in the ruptured regime. As the volume scales with R^3, we can deduce from the ideal gas law that a change in the ambient pressure of 3% is sufficient to obtain a decrease of 1% in R_0 and therefore a dramatic change in the bubble behavior. The change in "compression-only" and subharmonic behavior caused by a small change in the ambient pressure has been shown recently by Frinking et al. (2010).

Shell elasticity

In this work, we found a single value of the shell elasticity $\chi=2.5$ N/m for all bubbles. Previous experimental work also reports values of the shell elasticity and a typical value of $\chi=0.5-1$ N/m was found by several authors (Gorce et al. 2000; Van der Meer et al. 2007; Chetty et al. 2008). The reason for the apparent mismatch lies in the applicability of the linear viscoelastic shell model. The typical amplitude of oscillation A_1 in earlier work was in the order of 0.1. We show (see *e.g.* Fig. 10) that at an oscillation amplitude of $A_1 > 0.01$, the bubble is no longer oscillating purely in the elastic regime. A linear fit to the system that would partly oscillate in the buckled regime would therefore lead to an effectively lower shell elasticity. Moreover, the shell elasticity would then also be pressure dependent and the effective shell elasticity would decrease even more with increasing driving pressure.

Shell viscosity

While the effect of the shell elasticity is most pronounced in the shift of the resonance frequency, the effect of the shell viscosity is significant for the overall oscillation amplitude as a result of increased damping. In this article, we show that the relative amplitude of oscillation A_1 is well predicted with a constant shell viscosity $\kappa_s=6\cdot10^{-9}$ kg/s. With the linear viscoelastic model of De Jong et al. (1994), Gorce et al. (2000) found a shell friction parameter $S_f=0.45\cdot10^{-6}$ kg/s, which corresponds to a shell viscosity $\kappa_s=9\cdot10^{-9}$ kg/s. Chetty et al. (2008) used the model described by (Hoff et al. (2000). The authors used a shell viscosity $\mu_s=1$ Pas and a shell thickness $d_s=2.5$ nm and by taking $R=R_0$, the shell viscosity is recalculated $\kappa_s=8\cdot10^{-9}$ kg/s. Van der Meer et al. (2007) obtained the shell viscosity from the width of the measured resonance curves and found shell viscosities in the same order. Therefore, all values of the viscosity of these type of bubbles seem to correspond very well.

A *R(t)*-curve gives detailed information of the bubble response at a single applied frequency and pressure. The effect of shell viscous damping is visible in two ways: in the forced system, as said before, through an overall decrease of the oscillation amplitude, in the unforced system through an exponential decay of the bubble response. Figure 13 shows an experimental *R(t)*-curve (blue) and its corresponding simulation (red) of a 3.2 μm radius bubble insonified with a pressure $P_a=25$ kPa and a frequency $f=1.5$ MHz. The maximum amplitude of oscillation is very well predicted by the simulations using a shell viscosity $\kappa_s=6\cdot10^{-9}$ kg/s. On the other hand, this value of the shell viscosity predicts oscillations that decay gradually to zero after the ultrasound has been switched off, while these oscillations are not observed experimentally. Van der Meer et al. (2007) found a decrease in the dilation viscosity of the coating with increasing dilation rate, which could support the above observations. Furthermore, it is expected that also the shell viscosity of the coating depends on the actual state of the shell, *i.e.*, whether it is in the elastic, the buckled, or the ruptured regime. Adaptation of the model to account for a varying shell viscosity would add an improved level of sophistication to the shell-buckling model. On the other hand, these corrections may in the end prove to be of limited value for the medical imaging

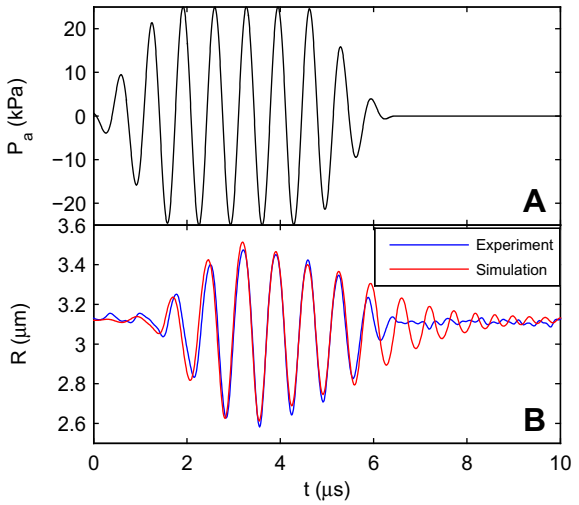

Fig. 13. (A) Applied acoustic pressure, P_a=25 kPa and f=1.5 MHz. (B) Comparison of an experimental $R(t)$-curve (blue) with a simulated $R(t)$-curve (red). The shell parameters are χ=2.5 N/m, $\kappa_s=6\cdot10^{-9}$ kg/s and $\sigma(R_0)$=0.02 N/m.

applications, as opposed to the nonlinear phenomena induced by the elastic, the buckled and the ruptured regime.

CONCLUSIONS

We have studied experimentally the resonance curves of individual ultrasound contrast agent microbubbles as a function of the acoustic pressure. The experiments were performed by positioning the microbubbles with the aid of optical tweezers so that they can be regarded as if in an unbounded fluid. In this way, we were able to exclude wall effects and isolate the influence of the phospholipid monolayer only. Coated microbubbles show strong nonlinear dynamics at low acoustic pressures, such as "compression-only" behavior and skewing of the resonance curve, which could not be predicted by models accounting for a linear viscoelastic shell. The model by Marmottant et al. (2005) accounting for an elastic regime and including buckling and rupture of the shell accurately predicts the observed nonlinear behavior of the phospholipid-coated microbubbles. We found that the dynamics of the BR-14 microbubbles can be explained with a single shell elasticity χ=2.5 N/m independent of the bubble radius. The maximum amplitude response of the bubbles is well predicted with a shell viscosity $\kappa_s=6\cdot10^{-9}$ kg/s.

In general, in the experiments the bubbles show more compression than expansion limiting the initial surface tension in the regime $0\leq\sigma(R_0)\leq\sigma_w/2$. Roughly, the observed phenomena can be divided into two regimes depending on the initial surface tension. A bubble initially in the buckled state shows strong compression-only behavior. The nondimensionalized frequency of maximum response is near 1.3 and almost independent of the acoustic pressure. A bubble initially in the elastic regime shows a rapid decrease of the frequency of maximum response with increasing acoustic pressure and a pronounced skewing of the resonance curves which we show is the origin of the so-called "thresholding" behavior.

The fundamental understanding of the nonlinear dynamics of phospholipid-coated bubbles at low acoustic pressures is important to optimize the frequencies and pressures used in the ultrasound imaging techniques. The model including buckling and rupture of the shell allows for the development of new imaging techniques using the observed phenomena of phospholipid-coated bubbles. For instance, elastic bubbles show "thresholding" behavior and are interesting for power modulation (Brock-Fisher et al. 1996) due to the nonlinear increase in the amplitude of oscillation with applied pressure. On the other hand, engineering of bubbles for specific techniques is a promising application. Stride et al. (2008) added nanoparticles to the shell restricting the bubbles from compression and to let them behave nonlinearly.

Further research on the influence of a phospholipid-coating on subharmonic behavior and on "compression-only" behavior of UCA microbubbles is conducted and described in detail in two upcoming papers by Sijl et al. (2010a, 2010b). Another exciting prospect is the development of ultra high-speed fluorescence imaging to visualize the time-resolved distribution of phospholipids at the interface during buckling and rupture of the shell (Gelderblom et al. 2010).

Acknowledgments—The authors would like to thank Timo Rozendal, Erik Gelderblom and Arjan van der Bos for help with the experiments and Pieter van der Deijl and Peter Eerkes for numerical simulations of the "thresholding" behavior. The authors acknowledge the technical assistance of Gert-Wim Bruggert, Martin Bos and Bas Benschop. The authors thank Bracco Research S.A. (Geneva, Switzerland) for discussions and for supplying the contrast agent BR-14. This work is partly financed by TAMIRUT a Specific Targeted Research (STReP) project supported by the 6th Framework Programme of the European Commission in the Nanosciences, Nanotechnologies, Materials and new Production Technologies area under contract number NMP4-CT-2005-016382.

REFERENCES

Borden MA, Longo ML. Dissolution behavior of lipid monolayer-coated, air-filled microbubbles: Effect of lipid hydrophobic chain length. Langmuir 2002;18:9225–9233.

Brenner MP, Hilgenfeldt S, Lohse D. Single-bubble sonoluminescence. Rev Modern Phys 2002;74:425–484.

Brock-Fisher GA, Poland MD, Rafter PG. 1996. Means for increasing sensitivity in non-linear ultrasound imaging systems. US Patent No. 5577505.

Chetty K, Stride E, Sennoga CA, Hajnal JV, Eckersley RJ. High-speed optical observations and simulation results of sonovue microbubbles at low-pressure insonation. IEEE Trans Ultrason Ferroelectr Freq Control 2008;55:1333–1342.

Chin CT, Lancée C, Borsboom J, Mastik F, Frijlink ME, De Jong N, Versluis M, Lohse D. Brandaris 128: A digital 25 million frames

per second camera with 128 highly sensitive frames. Rev Sci Instr 2003;74:5026–5034.

Church CC. The effects of an elastic solid surface layer on the radial pulsations of gas bubbles. J Acoust Soc Am 1995;97:1510–1521.

Crane JM, Hall SB. Rapid compression transforms interfacial monolayers of pulmonary surfactant. Biophys J 2001;80:1863–1872.

De Jong N, Cornet R, Lancée CT. Higher harmonics of vibrating gas-filled microspheres. Part one: Simulations. Ultrasonics 1994; 32:447–453.

De Jong N, Emmer M, Chin CT, Bouakaz A, Mastik F, Lohse D, Versluis M. "Compression-Only" behavior of phospholipid-coated contrast bubbles. Ultrasound Med Biol 2007;33:653–656.

Doinikov AA, Dayton PA. Maxwell rheological model for lipid-shelled ultrasound microbubble contrast agents. J Acoust Soc Am 2007;121: 3331–3340.

Emmer M, Van Wamel A, Goertz DE, De Jong N. The onset of microbubble vibration. Ultrasound Med Biol 2007;33:941–949.

Frinking PJA, Gaud E, Brochot J, Arditi M. Subharmonic scattering of phospholipid-shell microbubbles at low acoustic pressure amplitudes. IEEE Trans Ultrason Ferroelec Freq 2010;57:1762–1771.

Garbin V, Cojoc D, Ferrari E, Overvelde MLJ, Van der Meer S, De Jong N, Lohse D, Versluis M. Changes in microbubble dynamics near a boundary revealed by combined optical micromanipulation and high-speed imaging. Appl Phys Lett 2007;90:114103.

Garbin V, Cojoc D, Ferrari E, Proietti RZ, Cabrini S, Di Fabrizio E. Optical micro-manipulation using Laguerre-Gaussian beams. Jpn J Appl Phys 2005;44:5773–5776.

Gelderblom E, Kooiman K, Böhmer M, De Jong N, Lohse D, Versluis M. Ultra high-speed fluorescence imaging of ultrasound triggered local drug release. Proceedings of the European Symposium on Ultrasound Contrast Imaging 2010;15:82–84.

Gorce JM, Arditi M, Schneider M. Influence of bubble size distribution on the echogenicity of ultrasound contrast agents. Invest Radiol 2000;35:661–671.

Hilgenfeldt S, Lohse D, Zomack M. Response of bubbles to diagnostic ultrasound: a unifying theoretical approach. Eur Phys J B 1998;4: 247–255.

Hoff L, Sontum PC, Hovem JM. Oscillations of polymeric microbubbles: Effect of the encapsulating shell. J Acoust Soc Am 2000; 107:2272–2280.

Hope Simpson D, Chin CT, Burns PN. Pulse inversion Doppler: A new method for detecting nonlinear echoes from microbubble contrast agents. IEEE Trans Ultrason Ferroelectr Freq Control 1999;46: 372–382.

Klibanov AL. Microbubble contrast agents: Targeted ultrasound imaging and ultrasound-assisted drug-delivery applications. Invest Radiol 2006;41:354–362.

Lauterborn W. Numerical investigation of nonlinear oscillations of gas bubbles in liquids. J Acoust Soc Am 1976;59:283–293.

Lindner JR, Dayton PA, Coggins MP, Ley K, Song J, Ferrara K, Kaul S. Circulation 2000;102:531–538.

Lindner JR. Microbubbles in medical imaging: current applications and future directions. Nat Rev Drug Discov 2004;3:527–533.

Marmottant P, Van der Meer SM, Emmer M, Versluis M, De Jong N, Hilgenfeldt S, Lohse D. A model for large amplitude oscillations of coated bubbles accounting for buckling and rupture. J Acoust Soc Am 2005;118:3499–3505.

Plesset MS, Prosperetti A. Cavitation and bubble dynamics. Ann Rev Fluid Mech 1977;9:145–185.

Pocivavsek L, Dellsy R, Kern A, Johnson S, Lin B, Lee KYC, Cerda E. Stress and fold localization in thin elastic membranes. Science 2008; 320:912–916.

Prosperetti A. Nonlinear oscillations of gas bubbles in liquids: transient solutions and the connection between subharmonic signal and cavitation. J Acoust Soc Am 1975;57:810–821.

Sarkar K, Shi WT, Chatterjee D, Forsberg F. Characterization of ultrasound contrast microbubbles using in vitro experiments and viscous and viscoelastic interface models for encapsulation. J Acoust Soc Am 2005;118:539–550.

Sijl J, Dollet B, Overvelde M, Garbin V, Rozendal T, De Jong N, Lohse D, Versluis M. Subharmonic behavior of phospholipid-coated ultrasound contrast agent microbubbles. J Acoust Soc Am 2010a; in press.

Sijl J, Overvelde M, Dollet B, Garbin V, De Jong N, Lohse D, Versluis M. "Compression-only" behavior: A second order nonlinear response of ultrasound contrast agent microbubbles. J Acoust Soc Am 2010b; in press.

Stride E. The influence of surface adsorption on microbubble dynamics. Phil Trans R Soc A 2008;366:2103–2115.

Stride E, Pancholi K, Edirisinghe MJ, Samarasinghe S. Increasing the nonlinear character of microbubble oscillations at low acoustic pressures. J R Soc Interface 2008;5:807–811.

Unger EC, Hersh E, Vannan M, Matsunaga TO, McCreery T. Local drug and gene delivery through microbubbles. Prog Cardiovasc Dis 2001; 44:45–54.

Van der Meer SM, Dollet B, Chin CT, Bouakaz A, Voormolen M, De Jong N, Versluis M, Lohse D. Microbubble spectroscopy of ultrasound contrast agents. J Acoust Soc Am 2007;121:648–656.